---

**Article:**
Zhao, Y., Liu, Z. orcid.org/0000-0003-4533-252X, Zhang, H. et al. (3 more authors) (2024) On-line condition monitoring for rotor systems based on nonlinear data-driven modelling and model frequency analysis. Nonlinear Dynamics, 112. pp. 5229-5245. ISSN 0924-090X

https://doi.org/10.1007/s11071-024-09290-8

---

Nonlinear Dyn (2024) 112:5229–5245
https://doi.org/10.1007/s11071-024-09290-8

ORIGINAL PAPER

# On-line condition monitoring for rotor systems based on nonlinear data-driven modelling and model frequency analysis

**Yulai Zhao · Zepeng Liu · Hongxu Zhang · Qingkai Han · Yang Liu · Xuefei Wang**

Received: 6 July 2023 / Accepted: 27 December 2023 / Published online: 7 February 2024


**Abstract** This paper proposes a novel on-line rotor system condition monitoring approach using nonlinear data-driven modelling and model frequency analysis. First, the dynamic process model of the vibration transmission path between the vibration measurement points of two fulcrum structures is established by utilizing nonlinear data-driven modelling. Then, the unique frequency properties are extracted from the established model to reveal, in real time, the health condition of the rotor system. Finally, using the frequency properties as features, the unsupervised learning technology is applied to the on-line monitoring of the rotor system. Compared to conventional condition monitoring methods, the proposed approach can output an early warning 26 min before a shaft fracture occurs, without generating false alarms. Consequently, this approach can greatly enhance diagnostic accuracy, demonstrating its potential to contribute to the advancement of rotor system condition monitoring techniques.

**Keywords** Rotor systems · Nonlinear output frequency response functions · Dynamic process model · Condition monitoring

Y. Zhao · H. Zhang · Q. Han · Y. Liu
School of Mechanical Engineering and Automation, Northeastern University, Shenyang 110819, Liaoning, People's Republic of China

Z. Liu (✉)
Department of Automatic Control and Systems Engineering, The University of Sheffield, Sheffield S1 3JD, UK
e-mail: zepeng.liu@sheffield.ac.uk

X. Wang
School of Engineering, The University of Manchester, Manchester M13 9PL, UK

## 1 Introduction

For rotating machinery, such as an aero-engine, gas turbine, or machine tool [1], advanced and effective on-line condition monitoring methods are essential to detect the faults and deterioration of rotor systems, including shaft fractures, turbine disc cracks, rub-impact between the rotor and stator, and bearing spalling [2]. On-line condition monitoring is crucial to achieve the safe operation of rotor systems, reduce downtime and improve production efficiency [3].

Vibration analyses are widely used techniques for on-line monitoring of rotor systems because mechanical anomalies and faults generated from rotor systems can be collected from vibration signals [4, 5]. To conduct the on-line monitoring of rotor systems, one method is the signal feature-based technique, which directly extracts significant signal features, such as time-, frequency-, and time–frequency-domain features, from collected signals to determine the actual status of rotor systems. Then, based on the extracted signal features, supervised and unsupervised learning

methods are often performed to diagnose and prognose rotor systems [6]. For example, Liu [7] extracted the time- and frequency-domain features of shaft vibration signals, such as standard deviation, shape factor, root mean square frequency, and standard deviation frequency, and combined them with a non-fuzzy solution-weighted back-propagation-AdaBoost to realize a multi-fault diagnosis. Nath [8] combined distinctive frequency components, such as rotating frequency and its harmonic frequencies, in the vibration spectrum with a developed long short-term memory to diagnose the structural rotor fault. In addition, some scholars proposed to use fuzzy logic-based data preprocessing methods to reduce the influence of signal-based feature uncertainty on diagnosis results [9, 10]. However, signal feature-based methods still have two fundamental limitations and drawbacks:

(1) The primary concern is robustness. These methods are often limited to repeated and simple rotor rotation movements, which allows the signal features to accurately represent the condition of the rotor system. However, such methods may not be appropriate for practical applications where the rotor system is unbalanced or misaligned.
(2) For different working conditions, signal features may need to be re-designed, which makes the feature design a substantial task each time.

Another vibration analysis approach for on-line monitoring of rotor systems is the vibration displacement analysis-based method, which directly measures the vibration displacements of the shaft in two vertical directions using eddy current vibration sensors. Furthermore, condition monitoring can be conducted using orbit- or hologram-based methods [11]. For example, Nembhard [12] compared and analysed orbits under six conditions of added unbalance, bow, crack, looseness, misalignment, and rub-impact through experiments under four subcritical steady-state rotating speeds. Compared with the signal feature-based techniques, this method is more robust and simpler to use as no feature selection procedure is needed.

However, the vibration displacement analysis-based method requires the direct measurement of the rotor's condition, which places extremely high demands on the installation of the sensors. For some rotating machinery in real-world applications, such as the aero-engine, the position and number of sensor mounting points are limited because casing accessories are mostly set outside the rotor system [13], and vibration displacement signals of the shaft cannot be directly measured because no mounting points are near the shaft. For this kind of rotating machinery, the existing solutions of vibration analysis are mainly based on the vibration signal of the measurement point on the casing, and the rotating speeds related–frequency components of the vibration signals are determined to conduct spectrum analyses [14]. Nonetheless, this method is susceptible to interferences from the external noise, such as internal airflow excitation, casing and pipeline accessory vibration, and complex operating conditions with variable speed and load, which result in complex vibration responses, thus reducing the accuracy and stability of diagnosis [15]. Therefore, using the acquired vibration signals of the casing for monitoring the health status of the rotor system is a challenge, and applying the external vibration sensor to monitor the health status of this kind of rotor system to provide early warning for fault occurrence is a current research hotspot.

To fundamentally solve this issue faced by conventional vibration analysis techniques, in the present study, a novel diagnostic framework known as nonlinear data-driven modelling and model frequency analysis is proposed. Considering the dynamic coupling characteristics of the rotor system [16], the damaged bearing or shaft can affect the vibration response of the rotor system through the transmission path. The main idea of the proposed method is to build a dynamic process model through nonlinear data-driven modelling to reveal the dynamic characteristics of the rotor system. Then, model frequency analysis is conducted to extract the model frequency properties of the nonlinear data-driven model to evaluate the health conditions of the rotor system. Last, AI (artificial intelligence) methods are applied to use the frequency properties as features to conduct the on-line monitoring of the rotor system. The significance of this approach lies in its strong interpretability, namely the model frequency analysis can disclose unique and physically meaningful features of the rotor system. As previous studies demonstrated [17–19], the proposed diagnostic framework can be implemented for rotor systems monitoring. However, these studies simply utilized measured vibration displacement signals of the shaft, neglecting to consider the rotor system faults

associated with speed fluctuations, misalignment, and unbalance, which are impractical for real-world applications. This study is the first attempt to consider these challenges for monitoring rotor systems using the proposed approach, yielding results more representative of real-world applications. Promising results demonstrate that the proposed data-driven modelling and model frequency analysis surpass conventional monitoring methods, offering enhanced potential for industrial application.

The main contributions of this paper can therefore be summarized as follows:

(1) A run-to-failure experiment of a rotor system was conducted using a bearing-rotor test rig, wherein the shaft was operated from a healthy state to complete fatigue fractures. The life cycle test data of shaft fatigue fracture obtained from the test rig offer valuable insights and information for the study of on-line rotor system monitoring.
(2) Since this study conducted the run-to-failure experiment, more actual scenarios with more complicated faults that happened inside the rotor system are investigated.
(3) A novel on-line condition monitoring framework based on nonlinear data-driven modelling and model frequency analysis is proposed which outperforms the conventional monitoring methods in terms of reliability, robustness and accuracy.

The rest of this paper is organized as follows: In Sect. 2, the basic idea of using the vibration acceleration of fulcrum structures to monitor rotor systems is illustrated. The algorithm of nonlinear data-driven modelling and model frequency analysis is detailed introduced in Sect. 3. The implementation process of the proposed on-line condition monitoring approach is specified in Sect. 4. The experimental studies on the application of the proposed approach to the monitoring shaft degradation rotor systems are discussed in Sect. 5. Finally, conclusions are summarized in Sect. 6.

## 2 Basic principle of the proposed rotor system condition monitoring framework

For rotor systems shown in Fig. 1, such as aero-engines or gas turbines, vibration measurement points are generally arranged in an external casing close to the fulcrum structure to obtain maximum vibration energy. The greater the vibration energy of the measurement point, the more adequate the fault information will be. Therefore, using a vibration acceleration signal that is measured externally is worth studying to monitor the health condition of the internal rotor system.

As can be seen in Fig. 1, the vibration energy of the measurement point for this kind of rotor system is transmitted from the internal excitation source (regarded as power input), such as misalignment and disc unbalanced excitation. The power input generated by the disc finally reaches the vibration measurement point of the casing through the transmission path of the disc–shaft–bearing–fulcrum structure. When a component in the transmission path is damaged, such as a shaft misalignment or bearing spalling, the frequency properties of the transmission path system will change. Fault characteristics will affect the vibration response of the fulcrum structure through this transmission path. If the frequency properties can be determined by the vibration response of the measurement point, the health condition of the system can then be predicted.

As can be seen in Fig. 2, the variations, such as speed fluctuation, unbalance, misalignment, that occurred between two measurement points are regarded as the rotor system changes. Any situations that occurred outside the two measurement points are regarded as the environmental variations. In the present study, the external loading and working conditions are unvaried, so the environmental variations are unchanged. The objective of the present study is to implement transfer function-based diagnostic methods to monitor the system changes over time.

### 2.1 Justification of nonlinear data-driven modelling and model frequency analysis

As can be seen in Fig. 1, for the vibration response at both ends of any transmission path of rotor systems, the vibration response near the motor is defined as input signal $u(\varsigma)$, and the other end is defined as output signal $y(\varsigma)$; a general model representing the dynamics of the rotor system can be presented as

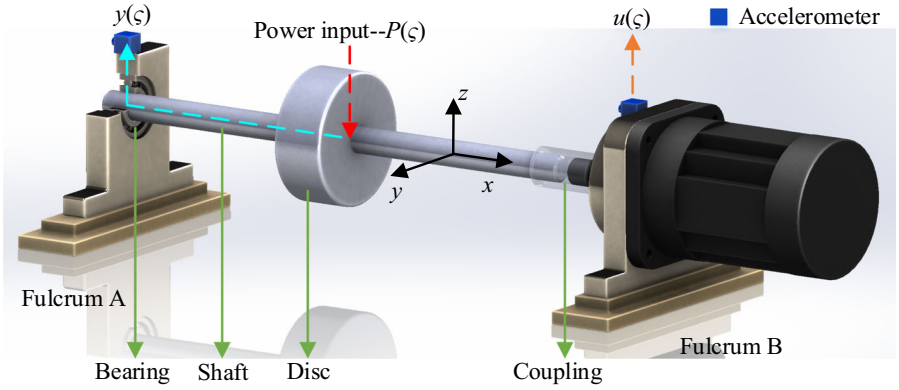


**Fig. 1** Typical vibration transmission path of rotor systems

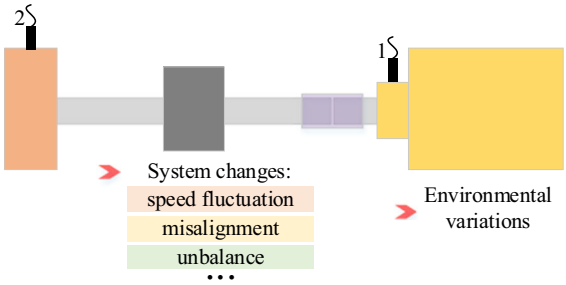


**Fig. 2** System changes and environmental variations

$$\begin{aligned} u(\varsigma) &= D_{(C_{1i})}[P(\varsigma)] \\ y(\varsigma) &= D_{(C_{2i})}[P(\varsigma)] \end{aligned} \tag{1}$$

where $P(\varsigma)$ represents the power input of the disc. Take an aero-engine as an example, the power input of the disc mainly comes from unbalance and airflow excitation. $D_{C1i}$ represents the dynamic characteristics of the transmission path between $u(\varsigma)$ and $P(\varsigma)$, and $D_{C2i}$ represents the dynamic characteristics of the transmission path between $y(\varsigma)$ and $P(\varsigma)$. $C_{1i}$ represents the components in the transmission path between $u(\varsigma)$ and $P(\varsigma)$. $C_{2i}$ represents the components in the transmission path between $y(\varsigma)$ and $P(\varsigma)$. $i$ is the number of components that included in the two transmission paths, such as the shaft and bearing shown in Fig. 1. Under the condition that $D_{C1i}$ and $D_{C2i}$ are invertible, Eq. (1) can be derived as

$$\begin{aligned} P(\varsigma) &= D^{-1}_{(C_{1i})}[u(\varsigma)] \\ P(\varsigma) &= D^{-1}_{(C_{2i})}[y(\varsigma)] \end{aligned} \tag{2}$$

which can be rewritten as

$$D^{-1}_{(C_{1i})}[u(\varsigma)] = D^{-1}_{(C_{2i})}[y(\varsigma)] \tag{3}$$

By transforming Eq. (3),

$$y(\varsigma) = D_{(C_{2i})}\left\{D^{-1}_{(C_{1i})}[u(\varsigma)]\right\} = D_{(C_{1i},C_{2i})}[u(\varsigma)] \tag{4}$$

In Eq. (4), if $D_{(C_{1i},C_{2i})}$ is a linear system, it can be transformed from the time domain into the frequency domain as

$$\frac{Y(\mathrm{j}\omega)}{U(\mathrm{j}\omega)} = \frac{\mathrm{FFT}[y(\varsigma)]}{\mathrm{FFT}[u(\varsigma)]} = \frac{\mathrm{FFT}\left\{D_{(C_{1i},C_{2i})}[u(\varsigma)]\right\}}{\mathrm{FFT}[u(\varsigma)]} = H(\mathrm{j}\omega) \tag{5}$$

where $H(\mathrm{j}\omega)$ represent the FRF (frequency response functions) of the transmission path between $u(\varsigma)$ and $y(\varsigma)$ reflecting the dynamics of the rotor system.

However, for the rotor systems in engineering, the dynamic relationship is generally nonlinear under the influence of assembly clearance, impact, or friction and other factors. The traditional linear FRF analysis simplifies the dynamic relationship $D_{(C_{1i},C_{2i})}$ into a linear system leading to the loss of a significant amount of fault information.

In addressing this issue, the present study develops a dynamic process model that accounts for nonlinear phenomena, utilizing a nonlinear data-driven approach. Subsequently, component faults and damage within the transmission path system are characterized by performing a nonlinear model frequency analysis. This analysis employs NOFRFs (nonlinear output frequency response functions), which extend traditional FRF to accommodate nonlinear cases. The following section will introduce the algorithms of

nonlinear data-driven modelling and subsequent model frequency analysis.

## 3 Algorithms of nonlinear data-driven modelling and model frequency analysis

### 3.1 Nonlinear data-driven modelling

(1) Model identification

In this paper, the nonlinear data-driven modelling employs the NARX (nonlinear autoregressive with exogenous input) model, which has the function of noise reduction and filtering and is convenient for subsequent frequency response analysis.

The purpose of nonlinear data-driven modelling is to obtain the dynamic relationship between two vibration measurement points as shown in Fig. 1. Let $u(k)$ and $y(k)$ be the discrete vibration signals collected from the continuous vibration signals $u(\varsigma)$ and $y(\varsigma)$, respectively, where $k$ represents the sampling point. The dynamic relationship can be represented by the NARX model with single input and single output in the discrete-time domain [20],

$$\begin{aligned} y(k) = F^{l}\big[&y(k-1), y(k-2), ..., y(k-\delta_y), \\ &u(k-1), u(k-2), ..., u(k-\delta_u)\big] + e(k) \end{aligned} \tag{6}$$

where $F^{l}[.]$ represents a nonlinear polynomial function with the maximum polynomial degree $l \in \mathrm{Z}^{+}$. $\delta_u$ and $\delta_y$ are the maximum lags for the two measure points signal, respectively. $e(k)$ represents the noise and unmodelled dynamics, which is an independent sequence and is normally defined as the prediction error term [20].

To facilitate the solving, rewriting Eq. (6) into the following matrix format,

$$y(k) = \sum_{m=1}^{M} \theta_m d_m(k) + e(k) \tag{7}$$

where $\theta_m (m = 1, 2, \ldots, M)$ represent the coefficients of the model terms, and $d_m(k)$ is the $m$th-order monomial term composed of $y(k\text{-}1)$, $y(k\text{-}2)$, $y(k\text{-}\delta_y)$,…, $u(k\text{-}1)$, $u(k\text{-}1)$, and $u(k\text{-}\delta_u)$. $M$ is the total number of candidate model terms, $M = (n + l)!/n!/l!$, and $n = \delta_y + \delta_u$.

To facilitate the solution, rewrite Eq. (7) into the following matrix form,

$$\begin{aligned} \mathbf{y} &= \mathbf{D}\theta + \mathbf{E} \\ &= \begin{bmatrix} d_1(1) & d_2(1) & \cdots & d_M(1) \\ d_1(2) & d_2(2) & \cdots & d_M(2) \\ \vdots & \vdots & \ddots & \vdots \\ d_1(N) & d_2(N) & \cdots & d_M(N) \end{bmatrix} \begin{bmatrix} \theta_1 \\ \theta_2 \\ \vdots \\ \theta_M \end{bmatrix} \\ &\quad + \begin{bmatrix} e_1 \\ e_2 \\ \vdots \\ e_M \end{bmatrix} \\ &= \begin{bmatrix} y_1 \\ y_2 \\ \vdots \\ y_M \end{bmatrix} \end{aligned} \tag{8}$$

where $\mathbf{y}$ is the vector of model output, $N$ is the total number of sampling points, $\boldsymbol{\theta}$ is a parameter vector, $\mathbf{D}$ is a dictionary matrix composed of the model candidate terms, and $\mathbf{E}$ is the modelling error vector.

The FROLS (forward regression with orthogonal least squares) introduced in Ref. [21] is applied to select the most significant model terms from the redundant initial dictionary matrix $\mathbf{D}$. The algorithm introduces the reordering process of model terms. Every step of the model terms search process will conduct a comprehensive screening of the remaining model terms and finally get a most concise model structure. The FROLS selected model can be determined as

$$\mathbf{y} = \mathbf{W}\alpha + \mathbf{E}^{*} \tag{9}$$

where $\mathbf{W}$ represents a final model structure, and $\mathbf{W} = \{\mathbf{d}_1, \ldots, \mathbf{d}_{M^*}\}$, $M^* << M$. $\boldsymbol{\alpha}$ is a FROLS parameter vector, $\boldsymbol{\alpha} = [\theta_1, \ldots, \theta_{M^*}]$, which can be calculated by [20]

$$\begin{aligned} \boldsymbol{\alpha} &= \arg\min\left\{ \|\mathbf{W}\alpha - \mathbf{y}\|_2^2 + \lambda\|\boldsymbol{\alpha}\|_2 \right\} \\ &= \left(\mathbf{W}^{\mathrm{T}}\mathbf{W} + \lambda\mathbf{I}\right)^{-1}\mathbf{W}^{\mathrm{T}}\mathbf{y} \end{aligned} \tag{10}$$

where $\lambda$ is the regularization parameter; and $\mathbf{I}$ is an $M^* \times M^*$ identity matrix. In this paper, the Euclidean norm is used to regularize the NARX model in order to meet the stability, robustness, and accuracy principles introduced in the following subsection. Although other methods can regularize the model, they are less efficient than the Euclidean norm in achieving these principles.

(2) Principles for choosing regularization parameter $\lambda$

To obtain a satisfactory NARX model, the regularization parameter $\lambda$ is a critical factor that determines the balance between bias and variance in the estimators obtained. During the tuning process of $\lambda$, it is necessary to consider three conditions to evaluate the generated models.

- *Stability*: To ensure that the model is stable, the MPO (model predicted output) predictions should be convergent. In MPO, the system output is initialized by a few known measured output values and then MPO is calculated from the identified model driven only by the given input [20]. For example, consider a NARX model,

$$y(k) = ay^2(k-1) + by(k-2) + cu(k-1) \tag{11}$$

The MPO predictions of the model are defined as

$$\begin{cases} \hat{y}(1) = y(1) \\ \hat{y}(2) = y(2) \\ \hat{y}(3) = a\hat{y}^2(2) + b\hat{y}(1) + c\hat{y}(2) \\ \hat{y}(4) = a\hat{y}^2(3) + b\hat{y}(2) + c\hat{y}(3) \\ \quad\vdots \quad\quad \vdots \quad\quad \vdots \quad\quad \vdots \\ \hat{y}(k) = a\hat{y}^2(k-1) + b\hat{y}(k-2) + c\hat{y}(k-1) \\ \quad\vdots \quad\quad \vdots \quad\quad \vdots \quad\quad \vdots \end{cases} \tag{12}$$

Due to the predicted values being on the right side, any prediction error will quickly accumulate and become obvious. In the event that the MPO predictions exhibit convergence, the candidate $\lambda$ will be utilized for subsequent verification. If the MPO predictions are divergent, the candidate $\lambda$ will be discarded.

- *Robustness*: Once the candidate $\lambda$ is selected from *Stability* principle, its robustness is assessed through $k$-fold cross-validation with the following process:

*Step 1* The original dataset is partitioned into $k$ subsets, and the modelling procedure is iterated $k$ times using the chosen candidate $\lambda$.

*Step 2* During each iteration, one of the $k$ subsets serves as the validation dataset, while the remaining $k-1$ subsets are combined to create a training dataset.

*Step 3* Ultimately, the MPO is assessed across all $k$ validation sets.

To evaluate the model's robustness, if any of the $k$ validation MPOs exhibit significant divergence, the candidate penalty parameter $\lambda$ will be excluded.

- *Accuracy*: After the candidate $\lambda$ is checked by *Stability* and *Robustness* principles, to ensure the accuracy of the model, the MSE (mean square error) is used to quantify the MPO predictions and make sure the accuracy of the model. The smaller the MSE is, the more accurate the model prediction will be. Under the condition that MSE meets the given precision, the principle of minimizing the number of NARX model terms should be followed.

$$\text{MSE} = (1/N)\sum_{k=1}^{N}(y(k) - \hat{y}(k))^2 \tag{13}$$

where$\hat{y}$ is the predicted output of the model. If the MPO predictions are convergent and MSE is satisfied, the $\lambda$ will be used for the modelling. Otherwise, the selected $\lambda$ will be abandoned.

(3) Optimization of parameter $\lambda$

To identify an appropriate $\lambda$ that satisfies the three key principles, an evolutionary algorithm is employed to seek the optimal regularization parameter $\lambda$ [19].

$$\mathbf{\Lambda}_i = \left[\lambda_{i,1}, \lambda_{i,2}, \ldots, \lambda_{i,r_i}, \ldots, \lambda_{i,R_i}\right] \tag{14}$$

where $\mathbf{\Lambda}_i$ represents a candidate parameter vector with a common difference $\psi/10^{i-1}$, where $\psi \in \mathrm{R}^+$ and $i \in \mathrm{Z}^+$. $1 \le r_i \le R_i$ and $\lambda_{i,r_i}$ indicates the candidate penalty parameter at the $i$th generation and the $r_i$th position, respectively. Based on this, the first vector is described as $\mathbf{\Lambda}_1 = \left[\lambda_{1,1}, \lambda_{1,2}, \ldots, \lambda_{1,r_1}, \ldots, \lambda_{1,R_1}\right]$ with the common difference $\psi$.

After that, the optimization process begins with the first iteration using $\mathbf{\Lambda}_i$ and applying the three principles. If no candidate penalty parameters in the first candidate parameter vector satisfies all three principles, $\mathbf{\Lambda}_i$ requires redesign. Otherwise, the potential penalty parameter can be selected as $\lambda_{1,r_1}$, and the corresponding MSE is denoted as $E_1$. Similarly, the second generation sequence is generated as $\mathbf{\Lambda}_2 = \left[\lambda_{2,1}, \lambda_{2,2}, \ldots, \lambda_{2,r_2}, \ldots, \lambda_{2,R_2}\right]$ with the common difference of $\psi/10$.

The evolution process is repeated, and the selected potential penalty parameter for the second iteration is $\lambda_{2,r_2}$ with the corresponding MSE of $E_2$. The evolution terminates at the $i$th evolution when $|1 - Ratio_{i,i\text{-}1}|$ is less than a predefined threshold $\rho$, which is a small number.

$$\left|1 - \text{Ratio}_{i,i-1}\right| \le \rho \tag{15}$$

where $\text{Ratio}_{i,i\text{-}1} = E_i/E_{i\text{-}1}$.

(4) Discussion on parameter choices

Before model identification, other suitable parameters need to be established, such as $l$, $\delta_u$, and $\delta_y$. The optimal $l$ can help to obtain satisfactory model terms. However, the increase of $l$ will significantly enlarge the size of the initial dictionary matrix $\mathbf{D}$. To improve the algorithm's solving speed, the initial $l$ is set to 2 for modelling. Similarly, the larger $\delta_u$ and $\delta_y$ can help in obtaining enough useful information for modelling but also generate redundant model terms, reducing computational efficiency. To obtain satisfactory $\delta_u$ and $\delta_y$, the trail-and-error method are adopted and combined with MSE above. Specifically, the combination of $\delta_u$ and $\delta_y$ that produces the smallest MSE will be used for subsequent dynamic process modelling.

### 3.2 Model frequency analysis

In the NARX modelling process, the NARX model meets the stability, robustness, and accuracy requirements through the selection and optimization of $\lambda$ to ensure the convergence. At this time, the NARX model's output in the time domain can be represented by a discrete Volterra series as [22]

$$\begin{aligned} y(t) &\approx \sum_{n=1}^{N} y_n(t) \\ &= \sum_{n=1}^{N} \int_{-\infty}^{+\infty} \cdots \int_{-\infty}^{+\infty} h_n(\tau_1 \cdots \tau_n) \prod_{i=1}^{n} u(t-\tau_i) d\tau_i \end{aligned} \tag{16}$$

where $N$ represents the maximum order of interest of the system's nonlinearity, and $h_n$ is the $n$th kernel function of the Volterra series. The convergence of the NARX model guarantees the convergence of the integrals in Eq. (16). In the frequency domain, the spectrum of the $n$th-order output $y_n(t)$ can be represented as

$$\begin{aligned} \text{FFT}(y_n(t)) = Y_n(\mathrm{j}\omega) = \frac{1/\sqrt{n}}{(2\pi)^{n-1}} \\ \int_{\omega_1+\cdots\omega_n=\omega} H_n(\mathrm{j}\omega_1, \cdots, \mathrm{j}\omega_n) \prod_{i=1}^{n} U(\mathrm{j}\omega_i) \mathrm{d}\sigma_{n\omega} \end{aligned} \tag{17}$$

Under the condition that $\text{FFT}(u_n(t)) = U_n(\mathrm{j}\omega) = \frac{1/\sqrt{n}}{(2\pi)^{n-1}} \int_{\omega_1+\cdots\omega_n=\omega} \prod_{i=1}^{n} U(\mathrm{j}\omega_i) \mathrm{d}\sigma_{n\omega} \neq 0$, the NOFRFs are defined as [22]

$$G_n(\mathrm{j}\omega) = \frac{\int_{\omega_1+\cdots\omega_n=\omega} H_n(\mathrm{j}\omega_1, \cdots, \mathrm{j}\omega_n) \prod_{i=1}^{n} U(\mathrm{j}\omega_i) \mathrm{d}\sigma_{n\omega}}{\int_{\omega_1+\cdots\omega_n=\omega} \prod_{i=1}^{n} U(\mathrm{j}\omega_i) \mathrm{d}\sigma_{n\omega}} \tag{18}$$

The $G_n(\mathrm{j}\omega)$ represents the result of a weighted sum of generalized frequency response functions (GFRF) $H_n(\mathrm{j}\omega_1, \ldots, \mathrm{j}\omega_n)$ over the $n$-dimensional hyper-plane $\omega = \omega_1 + \ldots + \omega_n$. Based on Eqs. (17) and (18), $n$th order NOFRF $G_n(\mathrm{j}\omega)$ can be represented as [22]

$$G_n(\mathrm{j}\omega) = \text{FFT}(y_n(t))/\text{FFT}(u_n(t)) = Y_n(\mathrm{j}\omega)/U_n(\mathrm{j}\omega) \tag{19}$$

where $u_n(t)$ and $y_n(t)$ are the $n$th order input and its corresponding output, respectively, and $u_n(t) = (u^*(t))^n$, $n = 1, \ldots, N$. $u^*(t)$ is the input excitation signal. At this time, the spectrum of the total output of the system (6) in the frequency domain can be represented as

$$\begin{aligned} \text{FFT}(y(t)) &= Y(\mathrm{j}\omega) \\ &\approx \sum_{n=1}^{N} Y_n(\mathrm{j}\omega) = \sum_{n=1}^{N} G_n(\mathrm{j}\omega) U_n(\mathrm{j}\omega) \end{aligned} \tag{20}$$

The discrete $n$th-order output $y_n(k)$ can be obtained using the Generalized Associated Linear Equations (GALEs) [23], which is defined as

$$\begin{aligned} &y_n(k) - \sum_{k_1=1}^{K} c_{1,0}(k_1) y_n(k-k_1) \\ &= \sum_{k_1,k_n=1}^{K} c_{0,n}(k_1, \cdots, k_n) \times \prod_{i=1}^{n} u(k-k_i) \\ &+ \sum_{q=1}^{n-1} \sum_{p=1}^{n-q} \sum_{k_1,\, k_{p+q}=1}^{K} c_{p,q}(k_1, \cdots, k_{p+q}) y_{n-q,p}^{\mathbf{K}}(k) \\ &\times \prod_{i=p+1}^{p+q} u(k-k_i) + \sum_{p=2}^{n} \sum_{k_1,\, k_p=1}^{K} c_{p,0}(k_1, \cdots, k_p) y_{n,p}^{\mathbf{K}}(k) \end{aligned} \tag{21}$$

where $n = 1, \ldots, N$, $\mathbf{K} = (k_1, \ldots, k_{p+q})$ is the integer set of delay for coefficients $c = (k_1, \ldots, k_{p+q})$, and

$$\begin{cases} y_{n,p}^{\mathbf{K}}(k) = \sum_{i=1}^{n-(p-1)} y_i(k-k_p) y_{n-i,p-1}^{\mathbf{K}}(k) \\ y_{n,1}^{\mathbf{K}}(k) = y_n(k-k_1) \end{cases} \tag{22}$$

The algorithms of the above nonlinear data-driven modelling and model frequency analysis algorithm are described as follows.

**Algorithm 1** Nonlinear data-driven modelling and model frequency analysis

**Input**: Input signal, **u**; output signal, **y**; input lag, $\delta_u$; output lag, $\delta_y$; polynomial degree $l$; excitation $\mathbf{u}^*$.

**Output**: The identified NARX model and NOFRFs $G_n(\mathrm{j}\omega)$, $n$=1, …, $N$.

1: Split the raw truncated signal into training and testing datasets.

2: Using the FROLS in Eq. (10) to identify the final model structure **W** using the training dataset.

3: Find a proper parameter $\lambda$ based on stability and accuracy criteria.

4: Based on the selected $\lambda$, the final identified NARX model can be obtained.

5: Determine the GALEs of the obtained NARX model from Eq. (21).

6: Solve the GALEs numerically and obtain the spectrum $Y_n(\mathrm{j}\omega)$, $n$=1, …, $N$.

7: Evaluate the NOFRFs $G_n(\mathrm{j}\omega)$, $n$=1, …, $N$, using Eq. (19).

Next, the Duffing equation is used as an example to illustrate the application of model frequency analysis in the condition assessment of nonlinear dynamic systems. Considering that the classical Duffing equation that has only a third stiffness term is not enough to represent the complex nonlinearity of the real mechanical system, this paper introduces a quadratic stiffness term into the classical Duffing equation. The Duffing equation with square stiffness term is established as follows:

$$m\ddot{y}(t) + c\dot{y}(t) + k_1 y(t) + \lambda k_2 y^2(t) + \lambda k_3 y^3(t) = u(t) \tag{23}$$

where $m$ and $c$ are the mass and the linear damping, respectively. $k_1$, $k_2$, and $k_3$ represent the linear stiffness, square stiffness, and cubic stiffness, respectively. $\lambda$ is the nonlinear factor, representing the strength of nonlinearity. The system nonlinearity can be increased by increasing $\lambda$, indicating that the system fault become serious. Equation (23) can be discretized to a NARX model using the forward-backwards difference (FBD) method [24] defined as

$$\begin{aligned} \dot{y}(t) &= \frac{y(t) - y(t-1)}{\Delta t} \\ \ddot{y}(t) &= \frac{y(t+1) - 2y(t) + y(t-1)}{\Delta t^2} \end{aligned} \tag{24}$$

where $\Delta t$ is the sampling period and $\Delta t = 1/f_s$,

$$\begin{aligned} y(t) =& c_{0,1}(0)u(t-1) + c_{1,0}(1)y(t-1) + c_{1,0}(2)y(t-2) \\ &+ c_{2,0}(1,1)y(t-1)^2 + c_{3,0}(1,1,1)y(t-1)^3 \end{aligned} \tag{25}$$

where the coefficients are represented as follows:

$$\begin{aligned} &c_{0,1}(0) = \Delta t^2/m, c_{1,0}(1) = (2m - c\Delta t - k_1\Delta t^2)/m, c_{1,0}(2) \\ &= (m - c\Delta t)/m, \\ &c_{2,0}(1,1) = -k_2\Delta t^2/m, c_{3,0}(1,1,1) = -k_3\Delta t^2/m \end{aligned}$$

Using the GALEs in Eq. (21), the first three order outputs expressions in time domain can be represented as,

$$\begin{cases} y_1(t) = c_{1,0}(1)y_1(t-1) + c_{1,0}(2)y_1(t-2) + c_{0,1}(1)u(t-1) \\ y_2(t) = c_{1,0}(1)y_2(t-1) + c_{1,0}(2)y_2(t-2) + c_{2,0}(1,1)y_1(t-1)^2 \\ y_3(t) = c_{1,0}(1)y_3(t-1) + c_{1,0}(2)y_3(t-2) + 2c_{2,0}(1,1)y_1(t-1)y_2(t-1) \\ \qquad + c_{3,0}(1,1,1)y_1(t-1)^3 \end{cases} \tag{26}$$

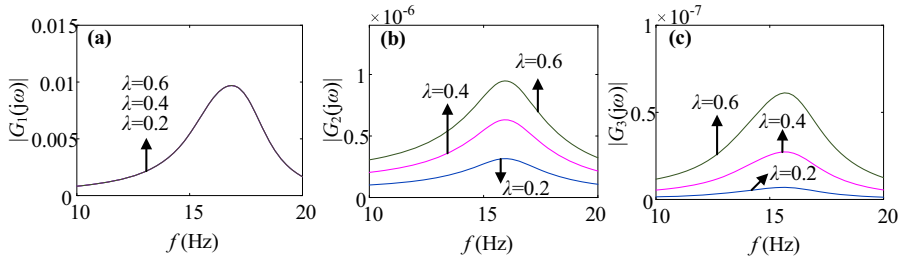


**Fig. 3** The NOFRFs under different nonlinear factor $\lambda$ **a** first NOFRF, **b** second NOFRF and **c** third NOFRF

Considering that the system is excited by the band-limited input,

$$u(t) = \frac{3}{2\pi}\frac{\sin(2\times 55\times \pi\times t) - \sin(2\times 30\times \pi\times t)}{t} \tag{27}$$

The parameters in Eq. (23) are set as $m = 1$ kg, $c = 20$ Ns/m, $k_1 = 1 \times 10^4$ N/m, $k_2 = 1 \times 10^7$ N/m$^2$, and $k_3 = 1 \times 10^9$ N/m$^3$, respectively. The sampling frequency is $f_s = 1/\Delta t = 5120$ Hz. Then, the vibration response of the system can be obtained by the Runge–Kutta numerical solving method. When the nonlinear factor takes three different values, namely $\lambda = \{0.2, 0.4, 0.6\}$, the first three orders NOFRFs of the system can be obtained as shown in Fig. 3.

As system nonlinearity increases caused by increasing the nonlinear factor $\lambda$, the first NOFRF, namely traditional FRFs (frequency response functions), remains the same, while the second and third NOFRFs increase significantly. The results indicate that the high-order NOFRFs obtained based on model frequency analysis can identify the faults occur and worsen that cannot be identified by traditional FRFs. For rotor systems, by comparing NOFRFs with a baseline, the dynamic characteristics can be monitored to achieve condition monitoring and fault diagnosis.

## 4 The implementation of the proposed on-line condition monitoring approach

The implementation of the proposed on-line health monitoring approach includes two main stages—off-line health state features extraction and on-line monitoring.

In the off-line stage, the NOFRFs features are extracted from the training set to construct the health state features via the following steps:

(1) Acquire the vibration acceleration of fulcrum structures under the initial health condition of rotor systems. Establish the NARX models characterising the health states using the vibration signals of the input and output measurement points. Use the FROLS algorithm to determine the model terms and their coefficients, and apply the stability and accuracy criteria to validate the model.

(2) Conduct the model frequency analysis using the identified models. Introduce the input excitation $u^*(t)$ with the continuous spectrum to calculate the models' NOFRFs ($G_n(\mathrm{j}\omega)$, $n = 1,\ldots, N$) using the GALEs in Eq. (21). Then, extract the amplitudes of the frequency components in the nonlinear spectrum within the bandwidth of input $(u^*(t))^n$, $n = 1, \ldots, N$, which are taken as the state features.

(3) Apply the $k$-means method to calculate the means of state features of all identified models in the training set, and take the means of state features as the health state features.

The on-line stage is the construction of the health indicator (HI), which mainly uses the vibration data collected under the current degradation state of the rotor systems with the following steps:

(1) Acquire the vibration acceleration of fulcrum structures under the current degradation state (including validation and test sets) to establish the NARX model satisfying validity to characterize the system dynamic process.

(2) Calculate the NOFRFs features of the model and take them as degradation state features. Then, compute the Euclidean distance between degradation state features and health state features to characterize the similarity, and apply the Euclidean distance as the HI.

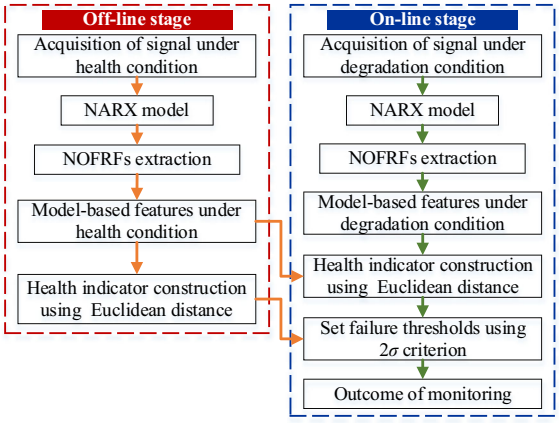


**Fig. 4** Flowchart of the proposed approach for on-line condition monitoring of rotor systems

$$\mathrm{HI} = \mathrm{D}(\mathbf{d}, \mathbf{h}) = \sqrt{\sum_{i=1}^{N} (d_i - h_i)^2} \tag{28}$$

where $N$ represents the number of feature elements, $d$ represents the current degradation state features, and $h$ represents the health state features.

(3) Set the hard failure threshold to $\mu + 2\sigma$ based on the $2\sigma$ criterion, where $\mu$ and $\sigma$ are the mean and standard deviation of the HIs of the training set, respectively. The moment when three consecutive HI points exceed the threshold is taken as the anomaly alarm. If only one or two points exceed the threshold and the next point falls below, the event is considered due to chance factors.

Figure 4 shows a schematic flowchart of the proposed off-line health state features extraction and on-line construction of HI and detection.

## 5 Shaft degradation monitoring

### 5.1 Experiment setup

To verify the feasibility of the proposed approach for rotor system condition monitoring based on the vibration signal of the fulcrum structure, the whole life cycle vibration data of the motor output shaft fatigue fracture were adopted. The structure of the bearing-rotor test rig was consistent with Fig. 1. One end of the shaft was connected with the output shaft of the motor by rigid coupling, and the ball bearing supported the other end. The non-driving end bearing housing and motor output shaft bearing sleeve were considered fulcrum structures. During the test rig assembly, the rotor system was adjusted to have an initial misalignment (out-of-line) of 0.1° to improve the motion instability and promote the fatigue cracks of the shaft and fracture occurrence [25, 26].

The primary measurement points were arranged as shown in Fig. 1. The vibration of the bearing sleeve of the motor output shaft was collected and defined as the input of the transmission path. The vibration of the bearing housing at the non-driving end was defined as the output of the transmission path. The overall transmission path was the motor output shaft bearing sleeve–motor bearing–shaft–coupling–shaft (disc)–support bearing–bearing housing. The failure or damage of any component in the transmission path would change the nonlinear frequency response function of the system.

Two BH5031EX-050-VL accelerometers with a sensitivity of 100 mV/g and a frequency range from 0.5 to 5 kHz were adopted. The sampling frequency was 12.8 kHz, and the vibration signal was collected for 1 s every 1 min. The motor drive speed was 1500 rpm. The shaft underwent completed breakdown after the experiment operated continuously for 316 min, and the data were collected for 316 s. Additionally, the axial vibration acceleration signals of two measurement points during the whole life cycle were combined to demonstrate the signal variations in the time domain (see Figs. 5 and 6). The vibration data from 0 to 90 min were used as the training set, the vibration data from 90 to 180 min made up the validation set, and the vibration data from 180 min to breakdown comprised the test set.

### 5.2 Nonlinear data-driven modelling

Considering the life cycle vibration data before the breakdown, 316 data segments 1 s long were acquired at each measurement point. Therefore, 316 NARX models were obtained using nonlinear data-driven modelling. For example, an identified NARX model using a training dataset is shown in Eq. (29) with the final selected parameters of $\lambda = 0.02$, $\delta_u = 5$, $\delta_y = 5$, and $l = 2$. The waveforms of real and predicted outputs are shown in Fig. 7, and the MSE is

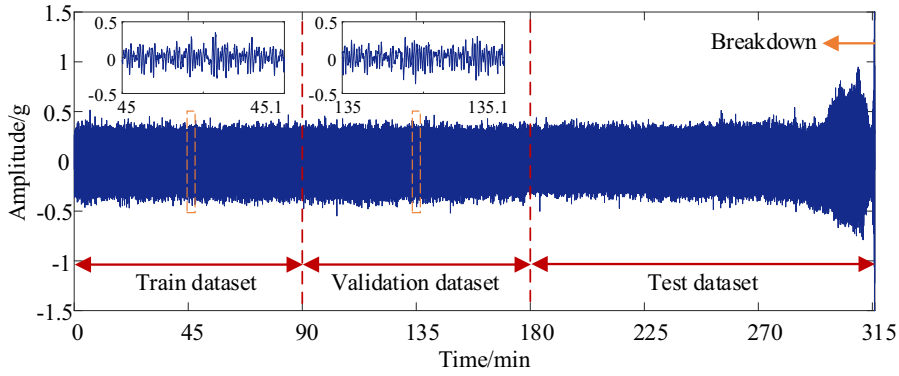


**Fig. 5** Vibration data of output measurement point under the whole life of shaft

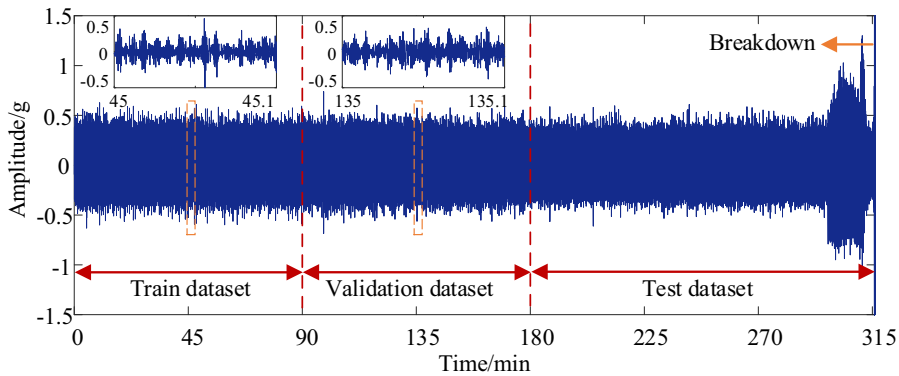


**Fig. 6** Vibration data of input measurement point under the whole life of shaft

0.00017, which means that the identified model can represent the nonlinear dynamics well.

$$\begin{aligned} y(k) = &-0.255966u(k-2) - 0.734631y(k-1) + 0.307441u(k-1) \\ &+ 0.235601u(k-4) - 0.284478y(k-2) - 0.098567y(k-3) \\ &+ 0.449025y(k-5) + 0.275088u(k-3) + 0.288734y(k-4) \\ &+ 0.009198u(k-3)y(k-4) + 0.004677u(k-1)u(k-4) + \ldots \end{aligned} \tag{29}$$

## 5.3 Model frequency analysis

Since the motor's output speed was set to 1500 rpm, the corresponding rotational frequency was 25 Hz. For the model frequency analysis, to observe the frequency properties at this frequency, the bandwidth of input excitation was set to 20–30 Hz to evaluate the NOFRFs of each model. (Usually, the motor speed is not strictly constant during rotation owing to changes in load and other unknown reasons, and the frequency range can be designed slightly wider to cover motor frequency variations.) The form of the input excitation is designed as

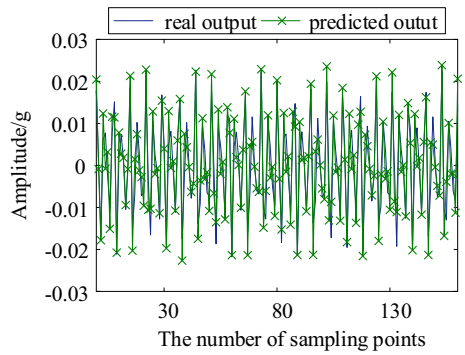


**Fig. 7** The real output and the predicted output of the identified NARX model

$$u^*(t) = \frac{1}{2\pi}\frac{\sin(20\times 2\times \pi\times t) - \sin(30\times 2\times \pi\times t)}{t}, \quad -2\text{s} \le t \le 2\text{s} \tag{30}$$

Based on Eq. (19), the NOFRFs of the identified NARX model are obtained. For this case study, the first three orders of NOFRFs were considered, and the

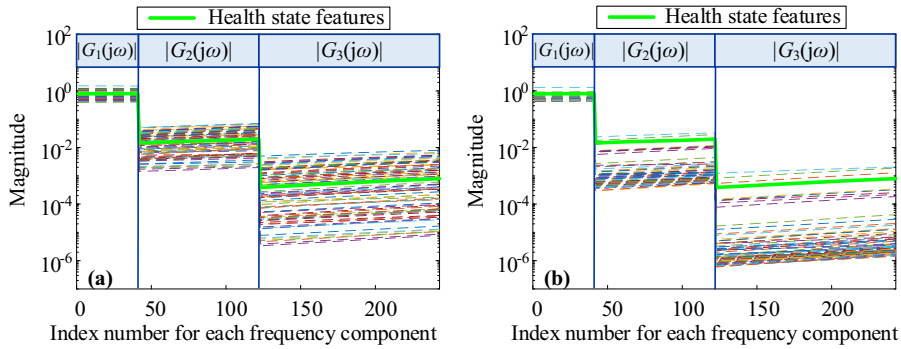


**Fig. 8** NOFRFs features of **a** training set and **b** validation set

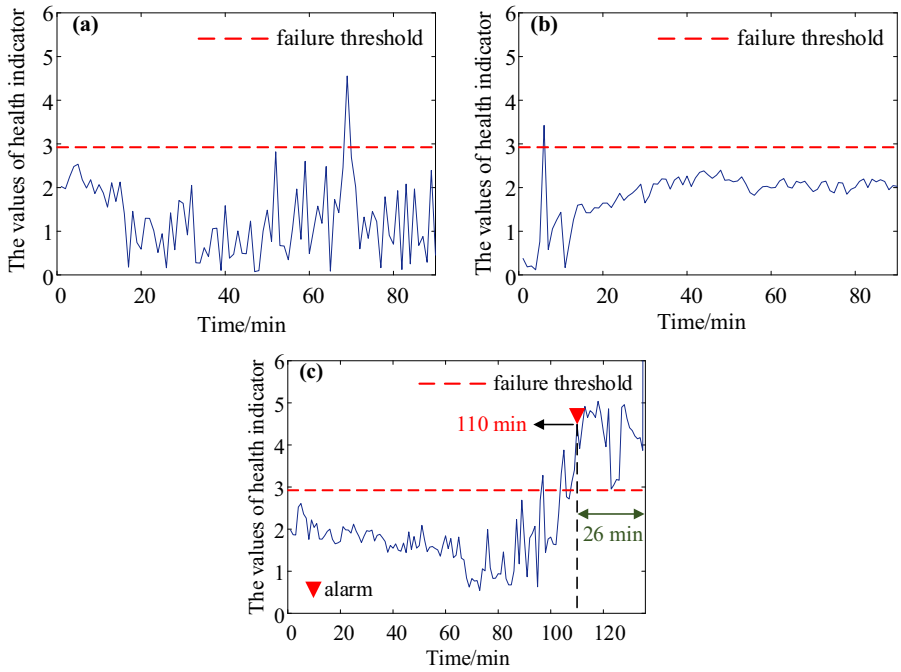


**Fig. 9** NOFRFs-based health indicator of **a** training set, **b** validation set, and **c** test set

amplitude of each frequency component was taken as the state features of the current moment.

### 5.4 Construction of health indicator and failure detection

The construction of the HI that reflects the health state of mechanical parts and quantifies the nonlinear degradation process is crucial to condition monitoring [27]. The obtained state features of the training set and validation set are shown in Fig. 8. As can be seen, the features are composed of first-order NOFRFs ($G_1$), second-order NOFRFs ($G_2$) and third-order NOFRFs ($G_3$). First, $G_1$ is derived from the fundamental frequency of the system having 40 frequency components as features. $G_2$ is derived from the first harmonic of the system where the number of the frequency components is 2 times the number of fundamental frequency components [20]. Therefore, the number of frequencies for the results of $G_2$ is 80 ($= 40 \times 2$). Similarly, $G_3$ is derived from the second harmonic of the system, so the number of frequencies for the results of $G_3$ is 120 ($= 40 \times 3$).

For the on-line construction of the HI, the $k$-means ($k = 1$) method is first used to calculate the mean of the state features of 90 data segments in the training set

and take them as the health state features, as shown in Fig. 8. After obtaining the health state features, the system's status can be analysed by calculating the similarity between the current degradation state features and the health state features. In this paper, based on Eq. (28), the Euclidean distance between the degradation and the health state features was calculated to characterize the similarity, and the distance was used as the HI. The value of the HI represents the change degree of the state features, and a noticeable change can indicate an anomaly. This interpretability lays a theoretical foundation for the engineering application of the proposed approach.

Finally, the failure threshold should be set. All state features of the training set were used to calculate the corresponding HI, as shown in Fig. 9a. The normal distribution test of the HI was conducted, and then, the failure threshold (red dash line in Fig. 9) was set to $\mu + 2\sigma$ according to the $2\sigma$ criterion to achieve a confidence interval of 95%, where $\mu$ is the HI mean in the training set and $\sigma$ is the standard deviation.

When the validation and test sets are used to detect the anomaly of the rotor system, the moment three consecutive points of the HI exceed the threshold is taken as the alarm. This is because $2\sigma$ criterion can achieve a confidence interval of 95%. If only one or two points exceed the threshold and the next point falls within it, the event is considered a chance factor. In Fig. 9b, only one HI point of the validation set exceeds the threshold, and the rest are below the threshold. Therefore, the validation set is in health status, consistent with reality. In Fig. 9c, the HI exceeds the threshold in the later period, where the marked point is the alarm time, which is 290 min of the life cycle. The breakdown occurs after 26 min, and thus, the NOFRFs-based HI can effectively warn the occurrence of shaft fatigue fracture.

### 5.5 Comparative study

To highlight the superiority of the proposed approach, the HIs based on traditional vibration signal features were calculated and compared with the proposed approach. The selected vibration signal features include the peak-to-peak value (PP), root mean square (RMS) [28], and amplitude of the rotational frequency

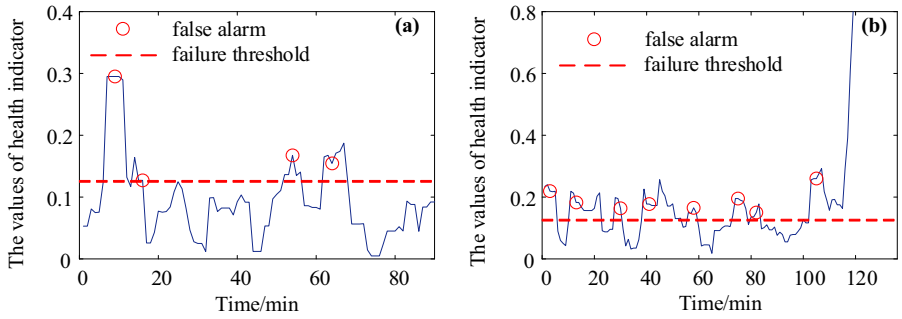


**Fig. 10** Peak-to-peak value-based health indicator of **a** validation and **b** test sets

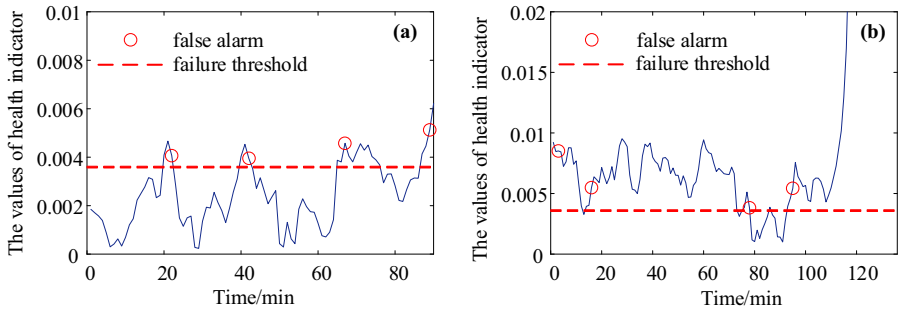


**Fig. 11** RMS-based health indicator of **a** validation **b** test sets

(ARF), which are commonly used signal features in the condition monitoring of rotor systems. Next, the three features of the vibration acceleration signals at the two measurement points were calculated respectively, and the HIs and failure thresholds were constructed using the same method. Additionally, the linear FRF-based HI and NARX model parameters (NARX-MP)-based HI [29] were also obtained and compared with NOFRFs-based HI. The linear FRF-based HI was generated using the FRF as the features, and this FRF was evaluated using the linear part of the NARX model output in relation to the linear input. The results are shown in Figs. 10, 11, 12, 13 and 14.

Then, by calculating the alarm times and the warning time of first alarm before the breakdown of the verification and test sets, the proposed HI is quantitatively compared with the traditional HIs. The comparison results are shown in Table 1.

For the validation set of the shaft fracture life cycle vibration data, the stability of the traditional vibration signal feature-based HIs was poor, and a false alarm appeared frequently. HIs based on PP and RMS had four false alarms at different times. Especially for the ARF-based HI, the continuous false alarm occurred within 30–80 min. For the test set, the alarm time was early and even at the beginning. After the alarm, the traditional vibration signal feature-based HIs would occasionally recover below the threshold. Still, most of the time, they were above the threshold, so they could not be used for shaft fracture condition monitoring.

Linear FRF-based HI had two false alarms for the validation set and most of HI values are above the threshold. For the test set, linear FRF-based HI are occasionally below the threshold in the later stages of degradation, meaning the unreliable alarms. Apart from two individual points, the other NARX-MP-based HIs are below the threshold value in the validation dataset. This means that the validation dataset is in a healthy status. In the test set, the NARX-MP-based HIs exhibit significant fluctuations, but still fail to meet the alarm requirement. This suggests that the shaft fracture cannot be predicted in advance. The results presented in Table 1 indicate that the traditional signal feature-based HIs and linear FRF-based HI had a high false alarm rate and unreliable warning

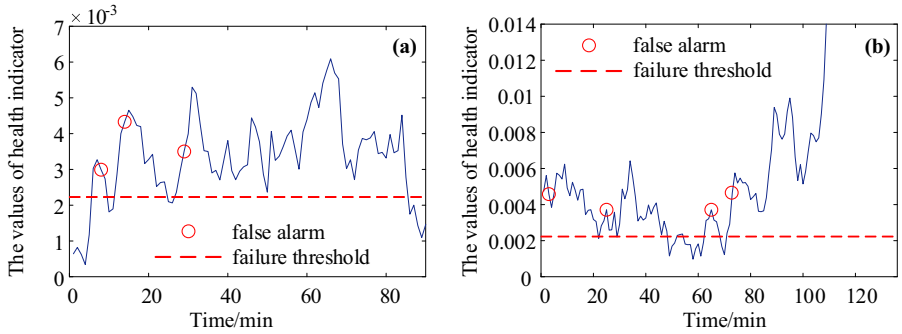


**Fig. 12** ARF-based health indicator of **a** validation and **b** test sets

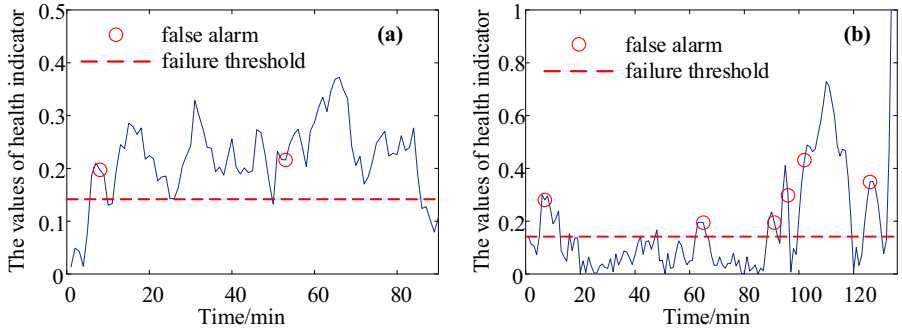


**Fig. 13** Linear FRF-based health indicator of **a** validation and **b** test sets

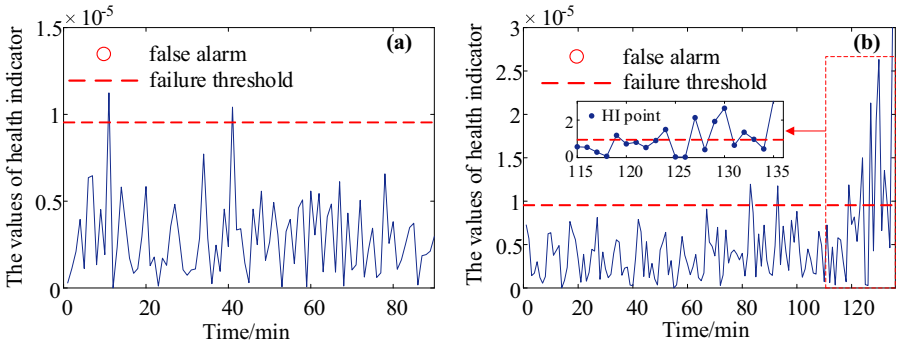


**Fig. 14** NARX-MP-based health indicator of **a** validation and **b** test sets

**Table 1** Comparisons of the proposed HI and traditional HIs

| Health indicators | Number of alarms | | Warning time (min) | |
|---|---|---|---|---|
| | Validation | Test | Validation | Test |
| NOFRFs-based HI | 0 | 1 | – | 26 |
| PP-based HI | 4 | 8 | 217 | 133 |
| RMS-based HI | 4 | 4 | 194 | 133 |
| ARF-based HI | 3 | 4 | 208 | 133 |
| Linear FRF-based HI | 2 | 7 | 218 | 129 |
| NARX-MP-based HI | 0 | 0 | – | – |

before the breakdown. Furthermore, NARX-MP-based HIs are unable to raise an alarm for shaft fracture, which further highlights the adaptability and reliability of the proposed HIs in the present study.

## 6 Discussion

To better illustrate the superiority of the proposed nonlinear data-driven modelling and model frequency analysis approach, some discussions are given as follows:

(1) *Reliability and robustness* Influenced by speed fluctuations, misalignment, and unbalance, the signal features, such as PP, RMS and ARF, change significantly, thus reducing the reliability of traditional signal feature-based monitoring methods. However, the proposed approach focuses on the frequency properties of the rotor system, which have the ability to resist these perturbations. Therefore, the proposed nonlinear data-driven modelling and model frequency analysis approach has better robustness and reliability.

(2) *Interpretability* The constructed HI and the on-line condition monitoring approach based on model frequency analysis have clear physical significance. The proposed approach assesses the health status of rotor systems by evaluating the variations of the NOFRFs of the systems' nonlinear data-driven model. However, the traditional signal feature-based monitoring methods only use statistic features which lack certain interpretability. With the complexity of mechanical equipment and operating conditions, the adaptability of traditional signal feature-based monitoring methods is seriously affected.

## 7 Conclusions

This study proposes an on-line condition monitoring approach for rotor systems based on nonlinear data-driven modelling and model frequency analysis. This proposed approach is validated using life cycle test data of shaft fatigue fracture obtained from a bearing-rotor test rig employing external vibration sensors,

specifically vibration acceleration of fulcrum structures, to monitor the health status of rotor systems. The results are more indicative of real-world applications, as they account for challenges related to speed fluctuations, misalignment, and unbalance. The results are more indicative of real-world applications, as they account for challenges related to external noise, such as noise from the motor rotation. Experimental results demonstrate that the proposed diagnostic method can effectively provide early warnings for shaft fatigue fractures while minimizing the occurrence of false alarms. Conversely, traditional methods based on vibration signal features exhibit a high false alarm rate, underscoring the superior robustness and adaptability of the proposed approach in comparison to conventional techniques.

Future research will focus on other types of mechanical failures to improve the practicality and universality of the proposed diagnostic framework, as well as how to increase the modelling speed and optimize the modelling process.

**Acknowledgements** This work was partially financially supported by the National Natural Science Foundation of China [grant No. 12072069].

**Funding** The funding was provided by the National Natural Science Foundation of China (Grant No 12072069).

**Data availability** The datasets generated and analysed during the current study are available from the corresponding author on reasonable request.

**Declarations**

**Conflict of interest** The authors declare that they have no conflict of interest concerning the publication of this manuscript.



## References

1. Wang, Y., Lei, Y., Li, N., Yan, T., Si, X.: Deep multisource parallel bilinear-fusion network for remaining useful life prediction of machinery. Reliab. Eng. Syst. Saf. **231**, 109006 (2023)
2. Wu, Z., Yan, H., Zhao, L., Yan, G., Chen, A., Hu, H., Zhang, W.: Influences of blade crack on the coupling characteristics in a bladed disk with elastic support. Aerosp. Sci. Technol. **133**, 108135 (2023)
3. Heng, A., Zhang, S., Tan, A., Mathew, J.: Rotating machinery prognostics: state of the art, challenges and opportunities. Mech. Syst. Signal Process. **23**(3), 724–739 (2009)
4. Zhao, Y., Wang, X., Han, S., Lin, J., Han, Q.: Fault diagnosis for abnormal wear of rolling element bearing fusing oil debris monitoring. Sensors **23**(7), 3402 (2023)
5. Chandra, N.H., Sekhar, A.S.: Fault detection in rotor bearing systems using time frequency techniques. Mech. Syst. Signal Process. **72**, 105–133 (2016)
6. Liu, R., Yang, B., Zio, E., Chen, X.: Artificial intelligence for fault diagnosis of rotating machinery: a review. Mech. Syst. Signal Process. **108**, 33–47 (2018)
7. Liu, Y., Zhao, C., Liang, H., Lu, H., Cui, N., Bao, K.: A rotor fault diagnosis method based on BP-Adaboost weighted by non-fuzzy solution coefficients. Measurement **196**, 111280 (2022)
8. Nath, A.G., Sharma, A., Udmale, S.S., Singh, S.K.: An early classification approach for improving structural rotor fault diagnosis. IEEE Trans. Instrum. Meas. **70**, 1–13 (2020)
9. Dotoli, M., Epicoco, N., Falagario, M., Sciancalepore, F.: A cross-efficiency fuzzy data envelopment analysis technique for performance evaluation of decision making units under uncertainty. Comput. Ind. Eng. **79**, 103–114 (2015)
10. Versaci, M., Angiulli, G., La Foresta, F., Crucitti, P., Laganá, F., Pellicanó, D., Palumbo, A.: Innovative soft computing techniques for the evaluation of the mechanical stress state of steel plates. In: International Conference on Applied Intelligence and Informatics, pp. 14–28. Springer Nature Switzerland, Cham (2022)
11. Liu, S., Qu, L.: A new field balancing method of rotor systems based on holospectrum and genetic algorithm. Appl. Soft Comput. **8**(1), 446–455 (2008)
12. Nembhard, A.D., Sinha, J.K., Yunusa-Kaltungo, A.: Experimental observations in the shaft orbits of relatively flexible machines with different rotor related faults. Measurement **75**, 320–337 (2015)
13. Hou, L., Cao, S., Gao, T., Wang, S.: Vibration signal model of an aero-engine rotor-casing system with a transfer path effect and rubbing. Measurement **141**, 429–441 (2019)
14. Nembhard, A.D., Sinha, J.K.: Unified Multi-speed analysis (UMA) for the condition monitoring of aero-engines. Mech. Syst. Signal Process. **64**, 84–99 (2015)
15. Zhang, X., Chen, G., Hao, T., He, Z.: Rolling bearing fault convolutional neural network diagnosis method based on casing signal. J. Mech. Sci. Technol. **34**, 2307–2316 (2020)
16. Xu, H., Yang, Y., Ma, H., Luo, Z., Li, X., Han, Q., Wen, B.: Vibration characteristics of bearing-rotor systems with inner ring dynamic misalignment. Int. J. Mech. Sci. **230**, 107536 (2022)

17. Zhu, Y., Zhao, Y., Lang, Z., Liu, Z., Liu, Y.: Online rotor systems condition monitoring using nonlinear output frequency response functions under harmonic excitations. IEEE Trans. Ind. Inf. **18**(10), 6798–6808 (2022)
18. Liu, Y., Liang, H.: Review on the application of the nonlinear output frequency response functions to mechanical fault diagnosis. IEEE Trans. Instrum. Meas. **72**, 1–12 (2023)
19. Liu, Y., Zhao, Y., Li, J., Ma, H., Yang, Q., Yan, X.: Application of weighted contribution rate of nonlinear output frequency response functions to rotor rub-impact. Mech. Syst. Signal Process. **136**, 106518 (2020)
20. Billings, S.A.: Nonlinear System Identification: NARMAX Methods in the Time, Frequency, and Spatio-Temporal Domains. Wiley, Hoboken, NJ, USA (2013)
21. Kadochnikova, A., Zhu, Y., Lang, Z., Kadirkamanathan, V.: Integrated identification of the nonlinear autoregressive models with exogenous inputs (narx) for engineering systems design. IEEE Trans. Control Syst. Technol. **31**(1), 394–401 (2022)
22. Lang, Z., Billings, S.A.: Energy transfer properties of nonlinear systems in the frequency domain. Int. J. Control. **78**(5), 345–362 (2005)
23. Zhu, Y., Lang, Z., Mao, H., Laalej, H.: Nonlinear output frequency response functions: a new evaluation approach and applications to railway and manufacturing systems' condition monitoring. Mech. Syst. Signal Process. **163**, 108179 (2022)
24. Li, Y., Luo, Z., He, F., Zhu, Y., Ge, X.: Modeling of rotating machinery: a novel frequency sweep system identification approach. J. Sound Vib. **494**, 115882 (2021)
25. Zhao, Y., Liu, Z., Lin, J., Han, Q., Liu, Y.: A novel nonlinear spectrum estimation method and its application in on-line condition assessment of bearing-rotor system. Measurement **221**, 113497 (2023)
26. Gómez, M.J., Castejón, C., García-Prada, J.C.: Automatic condition monitoring system for crack detection in rotating machinery. Reliab. Eng. Syst. Saf. **152**, 239–247 (2016)
27. Chang, M., Huang, X., Coolen, F.P., Coolen-Maturi, T.: Reliability analysis for systems based on degradation rates and hard failure thresholds changing with degradation levels. Reliab. Eng. Syst. Saf. **216**, 108007 (2021)
28. Li, N., Xu, P., Lei, Y., Cai, X., Kong, D.: A self-data-driven method for remaining useful life prediction of wind turbines considering continuously varying speeds. Mech. Syst. Signal Process. **165**, 108315 (2022)
29. Liu, Y., Zhang, L.: Data-driven fault identification of ageing wind turbine. In: 2022 UKACC 13th international conference on Control (CONTROL), pp. 183–188. IEEE (2022)